Electrostatic and Electromagnetic Turbulence Associated With the Earth's Bow Shock

PAUL RODRIGUEZ AND DONALD A. GURNETT

Department of Physics and Astronomy, University of Iowa, Iowa City, Iowa 52242

The electric and magnetic field spectral densities of plasma waves in the earth's bow shock have been measured in the frequency range 20 Hz to 200 kHz by using two 16-channel spectrum analyzers on the Imp 6 spacecraft. The electric field spectrum in the bow shock consists of two distinct components: one component has a broad peak typically centered between 200 and 800 Hz with an average (5.12-s time constant) spectral density at the peak of about 10^{-9} V^2 m^{-2} Hz^{-1}, and the other component increases monotonically with decreasing frequency approximately as $f^{-(2.0\pm0.5)}$ and has an average spectral density of about 3.0×10^{-9} V^2 m^{-2} Hz^{-1} at 36.0 Hz. The magnetic field spectrum in the shock has only one component that increases monotonically with decreasing frequency approximately as $f^{-(4.0\pm0.5)}$ and has an upper cutoff frequency near the local electron gyrofrequency. This magnetic field spectrum appears to be associated with the monotonic component of the electric field spectrum. The electric to magnetic energy density ratio ϵ_E/ϵ_B of this noise is about 10^{-3} to 10^{-4}, which is consistent with the energy density ratio expected for electromagnetic whistler mode waves in the bow shock. The broad peak in the electric field spectrum between 200 and 800 Hz has a large electric to magnetic energy density ratio, $\sim 10^2$ to 10^3, indicating that this component consists of almost purely electrostatic waves. Electrostatic noise with a spectrum similar to the turbulence in the shock but with lower intensities is observed throughout the magnetosheath region downstream of the shock. This magnetosheath electric field turbulence often includes many bursts with a distinct 'parabolic' frequency-time variation on a time scale of a few seconds. Spin modulation measurements of the electric field direction show that the electric field vectors in both the shock transition region and the magnetosheath region are preferentially oriented parallel to the static magnetic field direction. The electric field of upstream electron plasma oscillations also is oriented parallel to the static magnetic field.

A basic problem of shocks in collisionless plasmas is to identify and understand the dissipation mechanism that occurs in the transition region connecting the upstream and downstream states. In the absence of binary collisions, dissipation must occur through collective coulomb interactions of the charged particles. This results in the self-consistent generation of a turbulent spectrum of electrostatic waves that stochastically accelerates the charged particles. Experimentally, this is often described in terms of an 'anomalous' or effective resistivity for Ohm's law, $\mathbf{E} = \eta^*\mathbf{J}$, through which turbulent electric fields heat the plasma. The earth's bow shock provides a very convenient steady state laboratory for the study of high Mach number collisionless shocks. Electron and proton velocity distributions measured in the solar wind and magnetosheath near the bow shock indicate that strong thermalization occurs in relatively thin regions within the shock structure [*Montgomery et al.*, 1970; *Formisano and Hedgecock*, 1973*a*, *b*]. Magnetometer measurements of the magnetic field in the bow shock up to 10 Hz show a broad turbulent spectrum 2–3 orders of magnitude above the interplanetary spectrum [*Olson et al.*, 1969; *Holzer et al.*, 1966, 1972]. Electric field spectra in the range 560 Hz to 70 kHz [*Fredricks et al.*, 1968, 1970*a*, *b*] show electrostatic turbulence in the shock strongly correlated with magnetic field gradients, indicating the presence of some form of current-driven instability [*Wu and Fredricks*, 1972].

In this report we present some simultaneous measurements of electric and magnetic field spectral densities in the bow shock as obtained with the University of Iowa plasma wave experiment on the Imp 6 spacecraft. The frequency range of the plasma wave detector, 20 Hz to 200 kHz, covers most of the characteristic plasma frequencies for electrons and protons in average solar wind conditions. Electric fields are measured with long dipole antennas (~100 m tip to tip) with high sensitivity, of the order of 1 μV/m. Magnetic fields are measured with single-turn loop antennas.

The electric field measurements of *Fredricks et al.* [1968] were obtained with short dipole antennas (effective length of 0.5 m) on the Ogo 5 spacecraft, which are less sensitive than the long Imp 6 antennas (the ratio of effective lengths is ~100). To provide a basis for comparison between the Imp 6 and the Ogo 5 measurements, Imp 6 also has a short dipole antenna (effective length of 0.38 m).

The Imp 6 spacecraft was launched on March 13, 1971, with initial orbit parameters as follows: period, 4.18 days; perigee, 6614 km; apogee, 212,269 km (~34 R_e); inclination, 28.7°. The satellite is spin stabilized with its spin vector perpendicular to the ecliptic plane and pointing toward the south celestial pole and with a nominal spin period of 11.1 s.

The measurements of the present study were obtained during the first 30 orbits, covering the noon to dawn quadrant of local time. During this time, from March 17, 1971, to July 15, 1971, the solar wind conditions were usually relatively quiet with intermittent noisy periods as indicated by daily average values of *Kp*. The overall average *Kp* was about 2.0. In 30 orbits the spacecraft would have to cross the shock at least 60 times, but multiple crossings (due to the oscillatory motion of the bow shock structure past the spacecraft) have increased this number to over 150.

Experiment Description

Electric antennas. The spacecraft has three mutually perpendicular long dipole antennas identified in the spacecraft frame as $\pm X$, $\pm Y$, and $\pm Z$. The spacecraft spin vector is in the $+Z$ direction, and the X-Y plane is parallel to the ecliptic plane. The antennas are formed from prestressed conducting ribbons that assume a tubular shape as they are extended outward from the spacecraft. An insulating material covers all but the outer 16.8 m of the antennas. Extensions of the antennas

were made in seven steps over the time interval of the first nine orbits. The final tip-to-tip lengths are as follows: E_X = 54.0 m, E_Y = 93.2 m, and E_Z = 7.7 m. The effective lengths for the long antennas are taken as one-half the tip-to-tip lengths. The short dipole antenna is attached to the magnetometer boom and oriented in the Z direction. Two spherical wire cages at the ends of insulating rods form the elements of the short dipole antenna, its effective length thus being 0.38 m. This antenna was designed to serve as a backup to the long antennas and to provide the measurements at a different effective length.

Magnetic antennas. A system of three orthogonal loops at the end of a boom forms the magnetic antennas (M_X, M_Y, M_Z). They are oriented to conform to the coordinate system defined by the long electric antennas. Each loop is made of a single turn of aluminum tubing and has an area of 0.81 m^2.

Spectrum analyzers. Two 16-channel spectrum analyzers (A and B) are used to provide spectrum measurements. Each spectrum analyzer covers the frequency range from 20 Hz to 200 kHz with four filters per decade of frequency. The filter bandwidths range from about 20% of the center frequency at low frequencies to about 10% at high frequencies. Each filter is connected to a logarithmic receiver with 100-dB dynamic range and 10-μV sensitivity. The receiver output is proportional to the logarithm of the input voltage. By using the long electric antenna, electric fields as low as 0.2 μV/m can be detected. The magnetic field sensitivities depend on the wave frequency and range from 2.0 mγ at 36 Hz to about 10.0 $\mu\gamma$ at 16.5 kHz.

In the usual mode of operation, analyzer A is connected to the E_Y antenna, and analyzer B is connected to the M_X antenna. However, on command, each analyzer can be switched to any of the seven available antennas. In the high-rate data sampling mode the 32 analyzer channels are sampled in rapid sequence once every 5.12 s for average and peak outputs. The peak measurement gives the maximum receiver output over the 5.12-s interval between samples. The time constants are 5.12 s for the average measurement and 0.10 s for the peak measurement. A complete set of average and peak spectrum measurements is obtained for all channels once every 5.12 s and is called a snapshot. A snapshot is the basic data unit for the spectral density calculations presented in this paper. In addition to the spectrum measurements, there is a rapid-sample mode in which a given channel is sampled every 0.32 s. The rapid-sample measurements cycle through eight spectrum analyzer channels in a fixed sequence, 128 consecutive samples thus resulting from a given channel.

Shortly after launch it was determined that intense low-frequency (below 1 kHz) electric field interference was being produced by the spacecraft solar array. The main component of this noise is strongly spin modulated and is due to voltage transients caused by the shadow of the magnetic antenna boom and loops moving across the solar cell panels. The near 2:1 relationship between the spacecraft spin period (11.1 s) and the sampling interval (5.12 s) means that noise contamination in the peak measurements occurs in alternate snapshots and is easily identified.

Wide band receivers. Two wide band receivers provide broadband coverage over the ranges 10 Hz to 1 kHz and 650 Hz to 30 kHz. These analog signals are used to reconstruct analog frequency-time spectra for studying cutoffs, resonances, and other wave characteristics that require good frequency-time resolution.

PLASMA WAVE SPECTRA IN THE BOW SHOCK

General characteristics. Figure 1 illustrates the electric and magnetic field intensities typically observed in a bow shock crossing with the Imp 6 plasma wave experiment. Average and peak electric and magnetic field amplitudes are shown as a function of universal time for seven channels of both spectrum analyzers. The average field amplitudes are indicated by vertical lines, and the peak field amplitudes, by dots. The constant level for the peak measurements in the 36-Hz and 120-Hz electric field channels is caused by the previously mentioned interference from the solar array. The spacecraft crosses the bow shock, passing from the magnetosheath into the solar wind, at about 1048 UT, as is indicated by the sharp enhancement in the electric field strength above the average levels of both the magnetosheath and the solar wind at all frequencies below about 10.0 kHz. The electric field noise in the bow shock typically extends over a very broad frequency range, usually from 36.0 Hz, which is the lowest frequency measured, to greater than 10.0 kHz. In some cases, electric field noise associated with the bow shock has been detected up to 56.2 kHz.

The regions upstream and downstream of the bow shock are distinguished by their correspondingly low and high levels of electric field noise. In the magnetosheath the peak electric field spectral density in the 1.00-kHz and 3.11-kHz channels is typically about 3 orders of magnitude above the solar wind levels. In the solar wind the peak, and to a lesser extent the average, field strengths are strongly modulated at the lower frequencies by the solar array noise.

Immediately upstream of the bow shock a distinct enhancement is evident in the 31.1-kHz electric field strength from about 1048 UT to 1055 UT. This noise is primarily electrostatic, since no comparable enhancement is evident in the 31.1-kHz magnetic field data, and is caused by electron plasma oscillations at the local electron plasma frequency. Several accounts of electron plasma oscillations of this type, generated by electrons streaming into the solar wind from the bow shock, have been reported previously [*Fredricks et al.*, 1968; *Scarf et al.*, 1971; *Fredricks et al.*, 1971, 1972]. Electron plasma oscillations upstream of the bow shock are observed on almost all shock crossings with Imp 6.

Figure 1 shows only a slight increase in the magnetic field intensities at the bow shock. In the solar wind upstream of the bow shock the magnetic field intensities are below the sensitivity threshold of the receiver in all except the lowest-frequency channel. In the magnetosheath downstream of the bow shock, magnetic field fluctuations are evident in all frequency channels below about 1.00 kHz. These fluctuations are usually most evident in the peak measurements, indicating that the fluctuations occur on a time scale much less than the 5.12-s time constant for the average field strength measurements. Often the magnetic field measurements in the magnetosheath indicate turbulence at only two or three intermediate frequencies (such as 120 Hz and 200 Hz). The magnetosheath noise starts abruptly at the bow shock. The magnetic field fluctuations at the shock are usually only slightly larger than those in the magnetosheath.

Figure 2 shows a double crossing of the bow shock, the first at about 1251 UT and the second at about 1252 UT, caused by the oscillatory motion of the shock structure. A clean separation of the upstream and downstream regions by the shock transition occurs in this example, the upstream solar wind

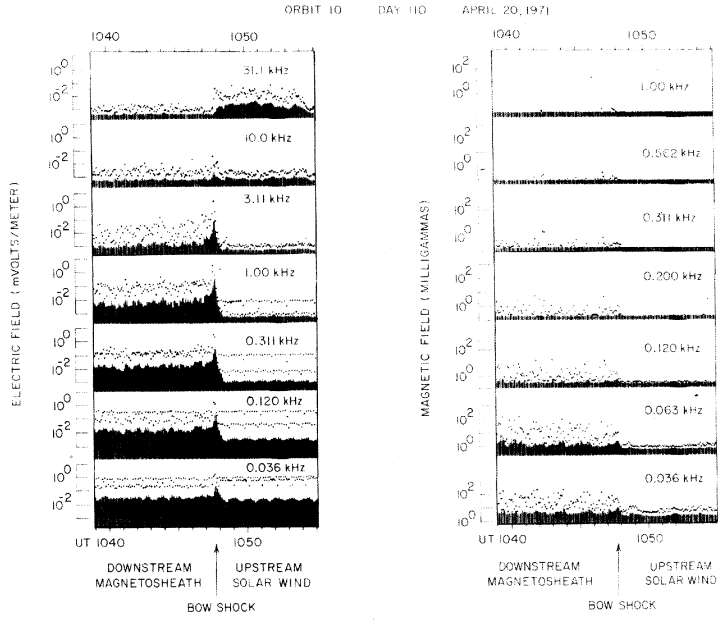

Fig. 1. A typical bow shock crossing as detected by the Imp 6 plasma wave experiment. Average measurements (5.12-s time constant) are plotted as vertical lines; peak measurements (0.1-s time constant) are plotted as dots. The shock transition occurs at about 1048 UT. The electric field measurements (left) show upstream plasma oscillations at 31.1 kHz after 1048 UT.

region being between 1251 and 1252 UT. The magnetic field measurements from the Goddard Space Flight Center (GSFC) magnetometer on Imp 6 show a clear jump in the magnetic field at each crossing from a steady upstream value, $B_1 \simeq 5\ \gamma$, to a downstream value, $B_2 \simeq 20\ \gamma$. The angle between the upstream field and the shock normal calculated from the model of *Fairfield* [1971] is $\psi(\mathbf{B}, \hat{n}) \simeq 92°$ for both crossings (D. Fairfield, personal communication, 1974). The bow shock in this case is therefore a perpendicular shock.

Electric and magnetic field spectral densities, $E^2(\omega)$ and $B^2(\omega)$, have been computed for 16 snapshots obtained for the second crossing of the shock shown in Figure 2. Each snapshot of data provides a complete electric and magnetic field spectrum for both average and peak measurements. The electric field strength is determined by dividing the measured ac voltage at the antenna terminals by one half of the tip-to-tip length, any antenna impedance corrections being ignored. The computed electric field spectral densities for the average field strength measurements are shown in the three-dimensional plot in Figure 3. The time axis is at an oblique angle in this plot, and successive spectra are 5.12 s apart. The time indicated at the bottom of the figure is the universal time of the first snapshot. For ease of reference, each spectrum is labeled by a snapshot number. Figure 4 shows the corresponding magnetic field spectra for the same time interval.

Beginning with snapshot 1 in Figure 3, strong electric field noise is present in the 16.5-kHz channel, which steadily decreases in magnitude as the shock is approached. This noise is the previously mentioned electrostatic electron plasma oscillations associated with electrons streaming into the solar wind from the bow shock. Low-frequency noise associated with the shock begins in snapshot 3 and steadily increases in intensity to a maximum in snapshot 7, by which time the electron plasma oscillations have disappeared. For the crossing at 1252 UT, the maximum rms electric field E_{rms} integrated across the entire frequency range, from 20 Hz to 200 kHz, occurs in snapshot 7 and has a value of 8.73×10^{-4} V m^{-1}. Up to 98% of the contribution to E_{rms} comes from below 1 kHz, and the spectrum has a broad maximum in the frequency range from about 200 Hz to 800 Hz. After the seventh snapshot the low-frequency noise decreases in magnitude, but the characteristic shape of the spectrum at the shock is maintained through the last snapshot in the figure. Examination of spectra taken when the spacecraft is well into the downstream magnetosheath region on this and other crossings reveals that the shape of the magnetosheath spectrum is the same as that of the shock except for variations in the low-frequency part of the spectrum. Thus the electric field spectrum in the shock appears to be carried into the downstream region. The downstream spectra also have a roughly periodic modulation of low-frequency intensities with a period of about four snapshots, or about 20 s. This modulation appears to be a general feature of the downstream electric field spectra near the bow shock. Periods range up to 60–70 s.

The magnetic field spectra in Figure 4 reveal the shock transition as merely an enhancement of low-frequency noise. Above about 3 kHz the spectral densities are close to or at the receiver noise level. The maximum rms magnetic field intensity

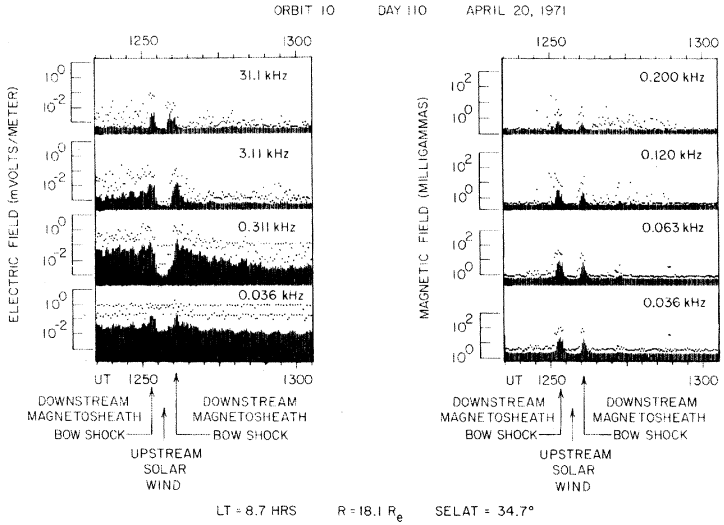

Fig. 2. A double crossing of the earth's bow shock as detected by the Imp 6 plasma wave experiment. The bow shock was very nearly a perpendicular shock during these crossings.

integrated across the entire frequency range, 20 Hz to 200 kHz, occurs in snapshot 6 and has a value of $5.49 \times 10^{-2}\ \gamma$. Most of the contribution to B_{rms} comes from below 100 Hz.

Electric and magnetic field spectra in the bow shock. For purposes of surveying the electric and magnetic field spectra for a large number of shock crossings, one spectrum that is representative of each shock crossing must be selected. The snapshot that gives the maximum rms field amplitude, found by using the average spectral density measurements integrated from 20 Hz to 200 kHz, is selected as the shock spectrum. The electric and magnetic field spectra thus selected are denoted by $E^2(\omega)_{sh}$ and $B^2(\omega)_{sh}$ and are referred to as the shock spectra.

A typical shock transition as resolved by the spectral measurements takes place over four or five snapshots, sometimes as many as 10. In the series of values of E_{rms} calculated for a given shock crossing there is usually only one maximum in E_{rms}, and thus $E^2(\omega)_{sh}$ is clearly defined. However, the series of values of B_{rms} calculated through the same shock crossing may have several maximums, none of which occur at the same time as the maximum in E_{rms}. For these cases we choose as the shock magnetic field spectrum the one that gives the largest value of B_{rms} within three snapshots of the shock electric field spectrum.

From the discussion above, it can be seen that our determination of the characteristic electric and magnetic field shock spectra is based on the snapshot in which the most intense low-frequency electric field noise occurs. We consider this to be appropriate, since the shock transition would be characterized by the spectrum $E^2(\omega)_{sh}$ that represents the greatest dissipation, i.e., the one with the greatest turbulent electric field energy density.

Figure 5 shows the shock electric field spectrum selected for the shock crossing at 1252 UT. This spectrum corresponds to snapshot 7 in Figure 3. Both the peak and the average electric field strengths obtained during this snapshot are shown. The noise level indicated in Figure 5 is the ambient noise level (both interference and natural noise) that existed in the solar wind just ahead of the shock. The shape of both the average and the peak electric field spectrum is characteristic of all the shock spectra examined in this study. However, as will be shown, the intensities at a given frequency vary over 2 orders of magnitude. The inflection in the spectrum, at about 200 Hz in Figure 5, sometimes becomes very pronounced, so that a broad peak develops in the spectrum between 200 and 800 Hz. The existence of a distinct peak in the spectrum suggests that this component of the electric field noise (indicated by the dashed curve in Figure 5) may result from a discrete noise source in the wave spectrum that is broadened by Doppler shifts and nonlinear interactions. The tendency for the electric field spectral density to continue to increase with decreasing frequency below about 100 Hz suggests that a second component also exists in the electric field spectrum varying approximately as f^{-2} (straight dashed line in Figure 5).

The electric field spectrum from the peak measurements in Figure 5 is from the same 5.12-s averaging period as the average measurements. The peak spectrum has approximately the same shape as the average spectrum but is shifted upward in intensity by about an order of magnitude. The large ratio between the peak and the average measurements indicates that the field strength has large (order of magnitude) fluctuations on a time scale less than the averaging time (5.12 s). The peak measurements give the upper bound on these fluctuations. For many shocks the peak spectrum does not have a smooth shape like that of the average spectrum but has a more irregular appearance with several sharp maximums. Most of these sharp maximums are grouped around two frequencies: one near the local electron plasma frequency in the upstream solar wind and the other near the broad peak in the average shock electric field spectrum.

Figure 6 shows the shock magnetic field spectrum selected for the shock crossing at 1252 UT in Figure 2. This spectrum corresponds to snapshot 6 in Figure 4; however, in accordance with our selection criterion, this shock spectrum does not correspond in time with the shock electric field spectrum, since in this case the maximum rms magnetic field intensity occurred slightly before (upstream of) the maximum rms electric field

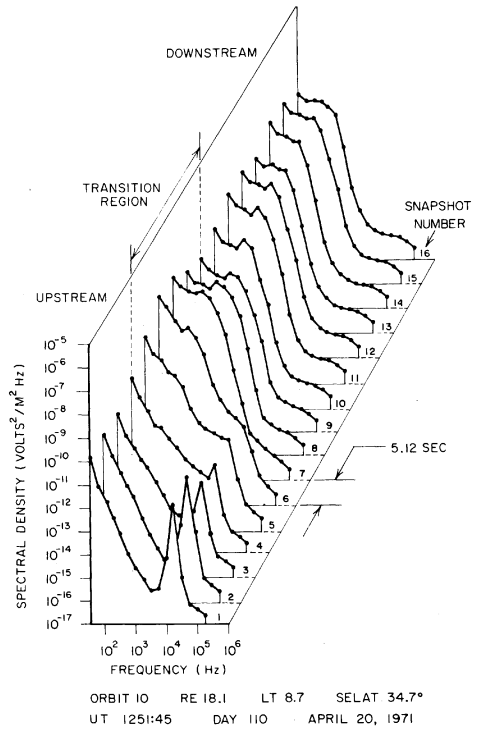

Fig. 3. The electric field spectra, based on average measurements, for the crossing at 1252 UT in Figure 2. The time indicated is for the first spectrum, and the averaging time of 5.12 s occurs between succeeding spectra thereafter. Snapshot 7 is the shock electric field spectrum.

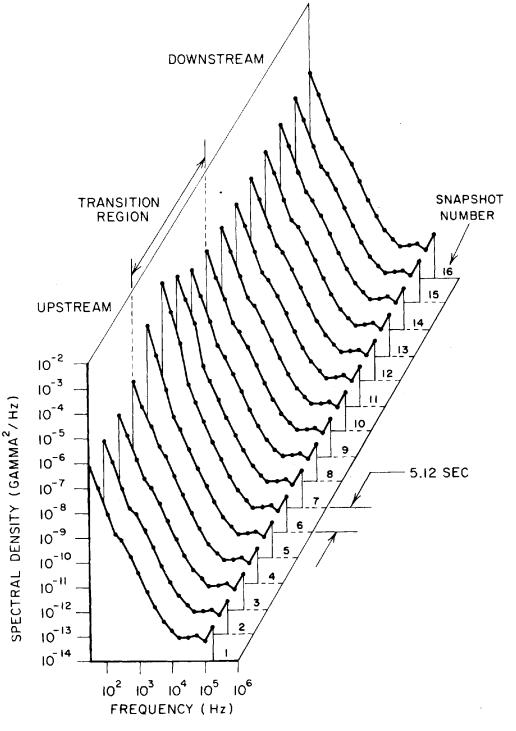

Fig. 4. The magnetic field spectra, based on average measurements, for the crossing at 1252 UT in Figure 2 and corresponding to the electric field spectra in Figure 3. Snapshot 6 is the shock magnetic field spectrum.

intensity. Both average and peak magnetic field spectra exhibit a generally smooth monotonic decrease with increasing frequency, varying approximately as f^{-4} in the range from 20 Hz to 200 Hz, with no evidence of a peak in the spectrum comparable to the peak in the electric field spectrum. A distinct steepening of the spectrum is also evident at a frequency of about 200 Hz. This steepening of the spectrum occurs at a frequency slightly below the local electron gyrofrequency, which in this case is about 350 Hz. The peak magnetic field spectral density is about an order of magnitude greater than the average magnetic field spectral density, indicating the presence of large fluctuations on a time scale less than 5.12 s.

In Figure 7 we have overlaid the peak and average electric field spectra $E^2(\omega)_{sh}$ for 36 shock crossings selected at random from the Imp 6 data to illustrate the range and variability of the electric field spectrum in the shock. In the majority of cases these spectra exhibit the spectral shape illustrated in Figure 5. Two distinct components are evident in the average electric field spectra and to a lesser extent in the peak spectra: at low frequencies one component decreases monotonically with increasing frequency approximately as $f^{-(2.0\pm0.5)}$, and the other component has a broad peak centered between 200 Hz and 800 Hz. The greatest variation in the spectral shape appears to occur in the spectra with the lowest intensities, ranging from spectra that decrease monotonically with no evidence of a peak to spectra that have a distinct peak that is displaced toward higher frequencies (~3 kHz). The largest intensity variation, which occurs in the range from about 200 Hz to 3 kHz, is associated with the broad peak in the spectrum. As the electric field intensity increases, starting from the lowest level, the peak initially becomes more pronounced until at an intermediate level the intensity of the monotonic component starts to increase and gradually merges with the broad peak. Except for the lowest intensities the main contribution to the rms electric field strength comes from the peak. As will be shown, the broad peak in the spectrum is caused by electrostatic waves, and the monotonic component is caused by electromagnetic whistler mode turbulence. In this study the largest rms electric field strength encountered from the peak measurements is 2.3×10^{-2} V m^{-1}. The largest rms electric field strength from the average measurements is 6.6×10^{-3} V m^{-1}.

Figure 8 shows the overlaid peak and average magnetic field spectra for the 36 shock crossings used in Figure 7. These spectra tend to show a monotonic decrease with increasing frequency, varying approximately as $f^{-(4.0\pm0.5)}$ in the range from about 30 Hz to 100 Hz with clear evidence of a steepening in the spectrum at about 100–200 Hz. This steepening in the magnetic field spectrum usually occurs slightly below the local electron gyrofrequency.

Electric to magnetic energy density ratio. To aid in identifying the plasma wave modes involved in the bow shock turbulence, we have investigated the electric to magnetic field

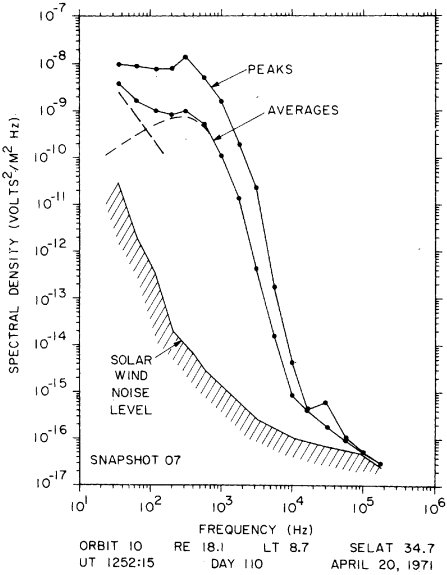

Fig. 5. The shock electric field spectrum $E^2(\omega)_{sh}$ selected on the basis of the rms electric field amplitude. The peak spectrum obtained during the averaging time of the average measurements is also shown. The two distinct components in the shock electric field spectrum are shown by dashed lines.

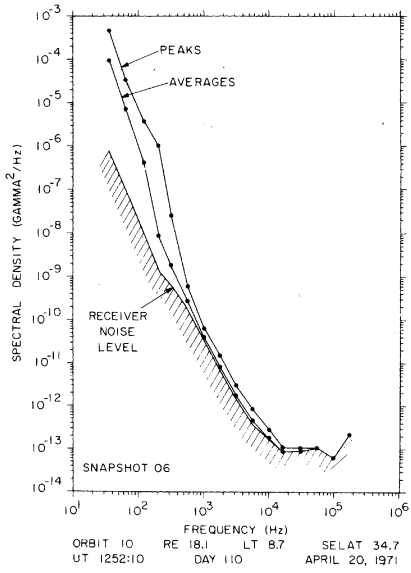

Fig. 6. The shock magnetic field spectrum $B^2(\omega)_{sh}$ for the shock crossing of 1252 UT. The characteristic frequency dependence f^{-4} is present in both the peak and the average spectrum. The spectrum steepens at about 200 Hz, below the local electron gyrofrequency at about 350 Hz.

energy density ratio as the spacecraft passes through a shock. Figure 9 shows the ratio of simultaneously measured energy densities ϵ_E/ϵ_B (where the energy densities are $\epsilon_E = E^2/8\pi$ and $\epsilon_B = B^2/8\pi$) at a sequence of snapshots for the shock crossing at 1252 UT in Figure 2. The snapshot numbers refer to the spectra of Figures 3 and 4. Because the magnetic field intensities at high frequencies (>3 kHz) are often comparable to or less than the receiver noise level, the magnetic energy densities must be corrected for the receiver noise level. Only magnetic field measurements that exceed the receiver noise level by at

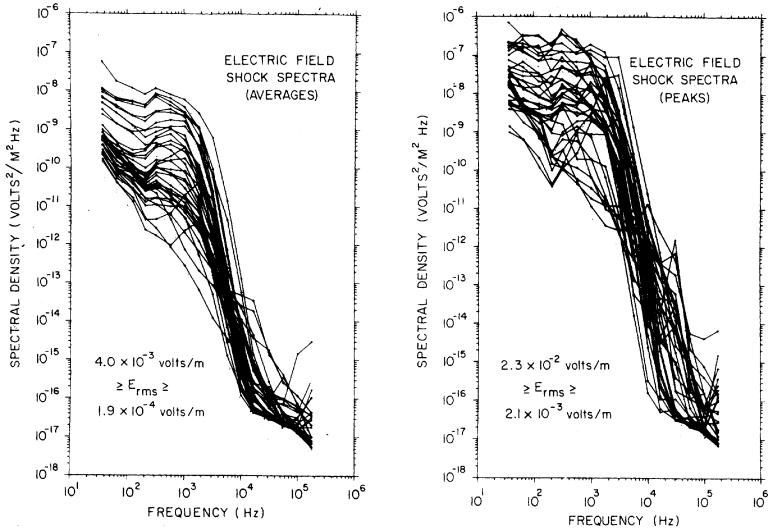

Fig. 7. A representative distribution of electric field shock spectra including average and peak measurements. The average spectra show that the broad peak in the electric field spectra becomes more distinct as the overall intensity of the spectra increases up to some intermediate range and then becomes less distinct as the very low frequency electric field spectral density saturates. The peak spectra are generally similar to the average spectra in shape but range up to an order of magnitude more in intensity.

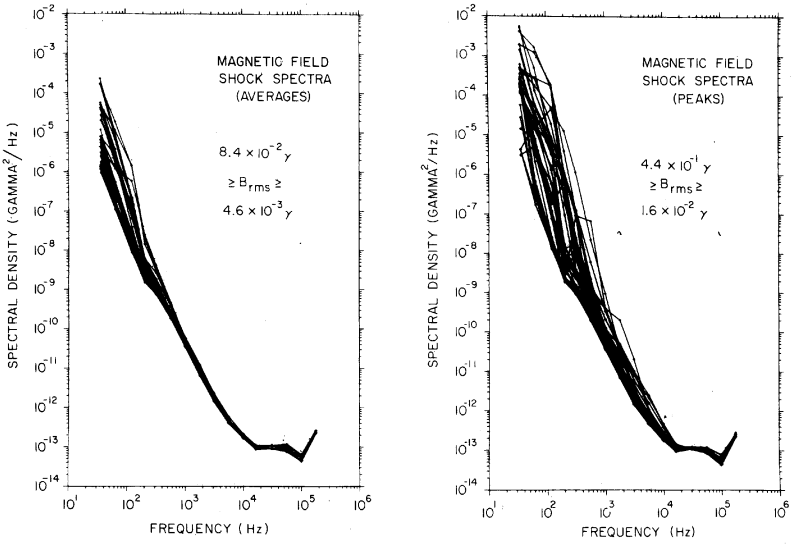

Fig. 8. Representative distribution of magnetic field shock spectra including average and peak measurements corresponding to the electric field spectra of Figure 7. Some of the peak spectra indicate the presence of distinct wave modes.

least two quantizing steps (0.8 dB) are used. At frequencies greater than about 10 kHz the magnetic field intensity is usually too small to be measured accurately, and so the energy density ratio cannot be determined at these high frequencies. As the spacecraft passes through the shock, a prominent peak develops in the energy density ratio at about 1 kHz. At snapshot 7, which is the time at which the most intense rms electric field occurs (Figure 3), the maximum energy density ratio is $\epsilon_E/\epsilon_B \simeq 5 \times 10^2$. This large ratio coincides in frequency with the broad peak in the electric field spectrum and indicates that this component of the spectrum consists of almost purely electrostatic waves.

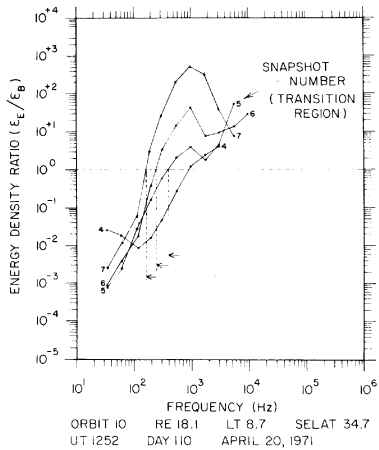

Fig. 9. The ratio of electric energy density to magnetic energy density for the shock crossing of 1252 UT in Figure 2. The low-frequency portion of snapshots 5, 6, and 7 is consistent with whistler waves. At higher frequencies, electrostatic noise is the dominant wave mode. The region of electrostatic noise is observed to broaden toward lower frequencies further into the transition region.

If we consider the lower-frequency limit of the electrostatic turbulence to be given by the frequency for which $\epsilon_E/\epsilon_B = 1$ (indicated by the horizontal broken line in Figure 9), it is seen that the electrostatic noise broadens toward lower frequencies as the electric field intensity increases. There is thus an indication that as the shock is traversed from the upstream side to the downstream side, the electrostatic turbulence first begins at high frequencies and is then transferred toward lower frequencies further into the transition region, where the main shock dissipation occurs. Only the increase to maximum intensity is shown in Figure 9, the decrease to the downstream state having approximately the same curves. At frequencies below about 120 Hz the energy density ratio remains approximately constant through the transition region, as it does in snapshots 5, 6, and 7, indicating that at these frequencies the shock turbulence involves a distinct electromagnetic mode.

To indicate the range and distribution of electric and magnetic energy density ratios in the bow shock, Figure 10 shows an overlay of the energy density ratio for 10 shock crossings selected at random. The simultaneous electric and magnetic field energy spectra used to calculate these ratios were selected on the basis of the maximum rms electric field intensity obtained from the average measurements. The energy density ratios for the shocks selected in Figure 10 show the same basic features evident for the single shock crossing in Figure 9. In the frequency range above about 200 Hz the electric field energy density exceeds the magnetic field energy density, sometimes by a factor of as much as 10^4, this feature confirming that the broad peak in the electric field spectrum consists of almost purely electrostatic waves. At frequencies below about 200 Hz the spectra with the lowest energy density ratio, in the range from 10^{-3} to 10^{-4}, show a distinct change in the slope, similar to that in snapshots 5, 6, and 7 in Figure 9. These energy density ratios correspond to the low-frequency

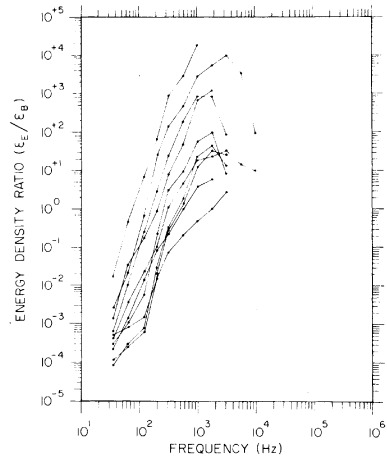

Fig. 10. A representative distribution of energy density ratios for 10 shock crossings selected at random from the shock electric and magnetic field spectra.

monotonic components of the electric and magnetic field spectra. In this frequency range the only electromagnetic wave that can propagate is in the whistler mode. The observed energy density ratios, 10^{-3} to 10^{-4}, are consistent with the electric to magnetic field ratio expected for whistler mode waves. The tendency for the energy density ratio to increase with increasing frequency, approximately proportional to $f^{1.5\pm0.5}$, is also consistent with the expected variation of the whistler mode refractive index, hence the electric to the magnetic field ratio, in this frequency range. The steepening of the magnetic field spectrum at $f \simeq 200$ Hz, evident in Figures 6 and 8, can be attributed to the whistler mode propagation cutoff at the local electron gyrofrequency. On the basis of this evidence we conclude that the low-frequency monotonic components of the electric and magnetic field spectra are caused by whistler mode turbulence generated in the bow shock.

High-resolution spectra. Wide band analog spectra of the shock crossings at 1251 and 1252 UT in Figure 2 are shown in Figure 11 for the range 0–500 Hz. The quiet upstream and turbulent downstream regions are clearly evident in the electric field spectrum. The shock transition region is most evident in the magnetic spectrum. Both the electric field spectrum and the magnetic field spectrum show a relatively unstructured noise enhancement in the shock transition. In the downstream region the electric field spectrum shows many 2- to 3-s bursts that have a distinct 'parabolic' frequency-time structure, sweeping rapidly downward in frequency from about 800 Hz, reaching a minimum of about 50 Hz, and then rapidly sweeping back upward in frequency. These parabola-shaped bursts are almost purely electrostatic, since no associated magnetic field is detected. They occur randomly in time and are characteristic of the downstream magnetosheath electric field spectrum. The distinctive frequency-time structure of these noise bursts has never previously been reported, and this electrostatic noise appears to represent a basic new turbulence dissipation mechanism operative in the magnetosheath. The time scale of these bursts is not resolved by the 5.12-s average measurements in the digital data of Figure 2; however, the peak measurements are indicative of the peak amplitude of the bursts.

An expanded time scale spectrogram of the shock crossing at 1252 UT is shown in Figure 12 for frequencies up to 1 kHz. The low-frequency electric field turbulence in the shock can be seen between 1252:10 and 1252:15 UT, corresponding to the time interval of snapshot 7 in Figure 5. The intense broad band electric field noise in the shock is clearly distinguished from the downstream region (after 1252:15 UT), in which a few parabola-shaped bursts are intermingled with the background noise. The most intense portion of the low-frequency magnetic noise occurs between 1252:00 and 1252:10 UT (corresponding to snapshot 6 of Figure 4) slightly upstream of the point where the most intense electric field noise occurs.

Electric Field Polarization

Since plasma waves are usually strongly influenced by the static magnetic field, it is important to establish the orientation of the wave electric field relative to the static magnetic field. The wave electric field direction, projected onto the plane of rotation of the electric antenna, can be determined from the modulation of the measured electric field amplitude due to the antenna rotation. A null in the measured electric field amplitude occurs when the antenna axis is perpendicular to the

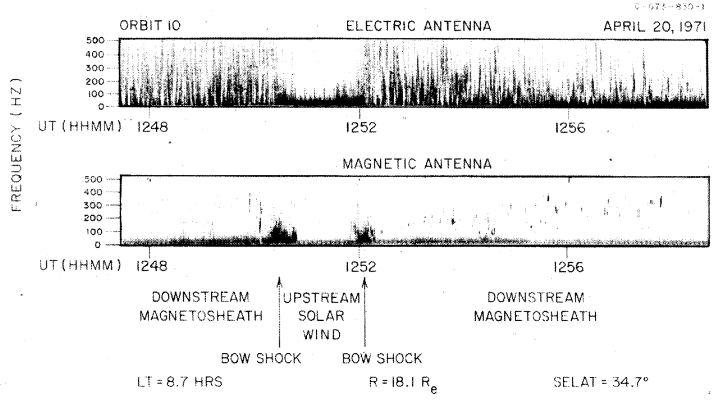

Fig. 11. Wide band spectra for the shock crossings of Figure 2 for frequencies 0–500 Hz. The turbulence of the shock transition appears more homogeneous than downstream turbulence for both the electric and the magnetic field. Discrete noise structure characterizes the downstream regions.

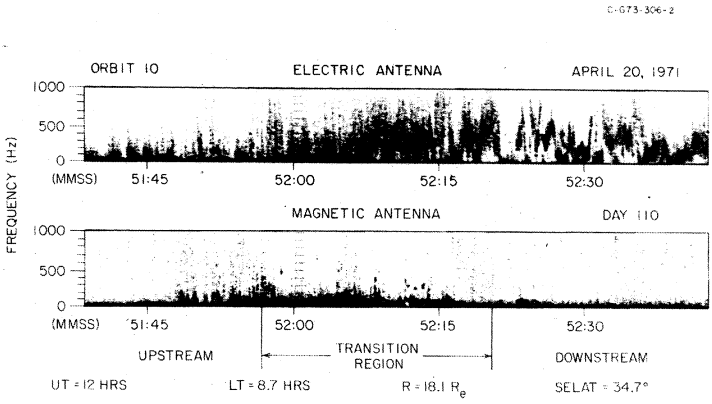

Fig. 12. Expanded time scale wide band spectra for the second shock crossing of Figures 2 and 11. The shock turbulence retains a homogeneous appearance, and the downstream noise shows a few parabola-shaped bursts in the electric field.

electric field direction, and a maximum occurs when the antenna axis is parallel to the electric field direction. Since high time resolution measurements are required, rapid-sample data must be used for this type of analysis.

This method of determining the electric field direction assumes that the noise intensity will remain nearly constant during at least one rotation (~11.1 s). For the upstream and downstream waves, which often have an approximately constant amplitude for many rotations, the electric field direction can be determined reliably by using this technique. Because the time required to traverse a shock is often comparable to the rotation period, it is more difficult to apply this technique to the noise that occurs in the shock. Only shock crossings that have an approximately constant amplitude for at least 10 s or more can be analyzed. The number of cases that can be analyzed is further restricted by the requirement that rapid-sample measurements must be available in the correct frequency channel for the event of interest.

Upstream electron plasma oscillations. Figure 13 shows an example of upstream electron plasma oscillations for which suitable rapid-sample measurements are available to determine the electric field direction. The electron plasma frequency in this case is estimated to be about 20 kHz. The spectrum of the plasma oscillations is sufficiently broad that moderate electric field intensities are evident in the 31.1-kHz channel throughout the entire region prior to the shock crossing at 1548:30 UT. The electrostatic noise labeled precursor at 3.11 kHz appears to be a component of the electron plasma oscillation spectrum that has broadened to frequencies well below the local electron plasma frequency about 5 min before the shock is encountered. Precursor effects of this type are frequently observed in association with the bow shock, usually starting a few minutes before the shock is encountered.

Two periods, labeled A and B, during which rapid-sample measurements were obtained are shown in Figure 13. The spin modulation of the electron plasma oscillations in the 31.1-kHz channel, starting at 1541:29 UT, is shown in the polar plot labeled A in Figure 13. The points shown in this polar plot are the electric field strengths obtained during the rapid-sample interval and plotted radially outward from the origin according to the logarithmic scale shown below the plot. The polar angle is the angle between the electric antenna axis and the satellite-sun line, measured counterclockwise as it is viewed from the north ecliptic pole (the spacecraft spin axis is perpendicular to the ecliptic plane). The static magnetic field direction, projected onto the ecliptic plane, is at an angle $\phi_B = 94°$, as is indicated by the dashed line in the polar plot. The magnetic field vector lies at an angle of 16° above the ecliptic plane.

The points shown in the polar plot include four complete rotations of the spacecraft. The electric field intensities have a pronounced maximum when the antenna axis is parallel to the projected magnetic field direction and a minimum when the antenna axis is perpendicular to the magnetic field. Since the magnetic field direction in this case is very close to the plane of rotation of the electric antenna (the ecliptic plane), it is evident that the electric field direction of the upstream electron plasma oscillations is parallel to the static magnetic field, as would be expected if these waves are excited by electrons streaming along the static magnetic field. Polar plot B in Figure 13 shows that the electric field direction of the precursor waves is also aligned parallel to the static magnetic field. Similar observations for other shock crossings with widely varying magnetic field directions show that the electric field direction of these upstream electron plasma oscillations is always parallel to the static magnetic field.

Electrostatic waves in the bow shock. In Figure 14 we show an example of the spin modulation observed for the electrostatic noise in the bow shock. The shock crossing in this case occurred near the ecliptic plane at 10.3 hours LT with very quiet upstream conditions. The GSFC magnetometer shows that the upstream magnetic field direction is very nearly perpendicular to the shock normal, $\psi(\mathbf{B}, \hat{n}) \simeq 87°$, so that the bow shock is a perpendicular shock. The electrostatic noise associated with the shock is near maximum intensity for one complete rotation, so that a definite spin modulation pattern can be obtained.

The detailed electric field amplitude obtained from the rapid-sample data in the 3.11-kHz electric field channel is shown as a function of time in the upper panel of Figure 14, and the polar plot corresponding to the interval between points *a* and *b* is shown in the lower panel. The electrostatic turbulence associated with the shock transition occurs between about 1440:37 and 1440:49 UT. In this same time interval the GSFC magnetometer data show the magnetic field increasing

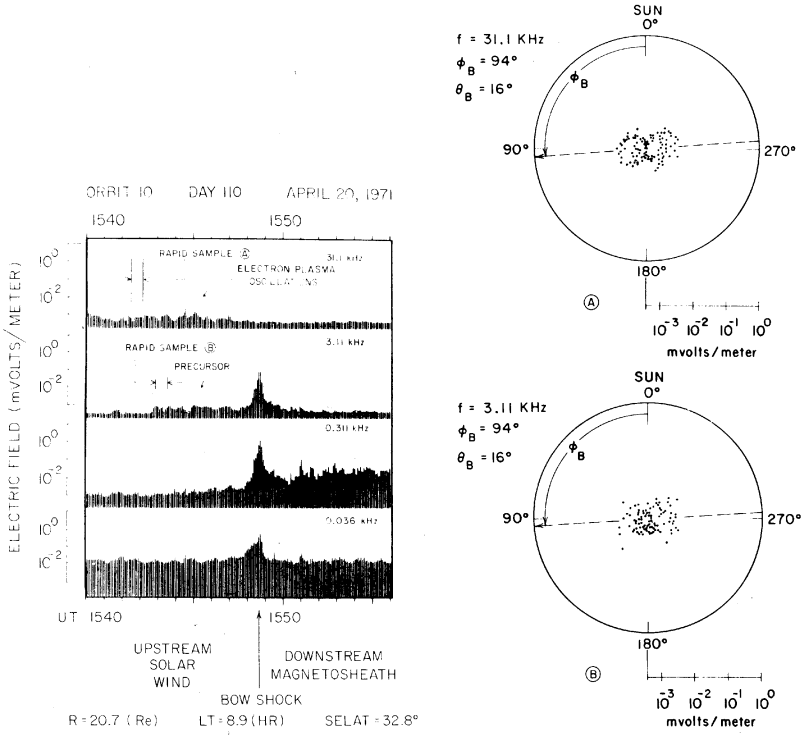

Fig. 13. Upstream electron plasma oscillations and precursor encountered a few minutes before the shock crossing at about 1548:30 UT. The rapid-sample measurements A and B give the spin-modulated electric field amplitudes shown in the two polar plots. The electric field vector of these waves is predominantly aligned parallel to the static magnetic field.

monotonically from about 12 γ to about 50 γ. The solar ecliptic longitude and latitude of the magnetic field direction remain constant at approximately $\phi_B = 255°$ and $\theta_B = 43°$, respectively, through the transition. The magnetic field direction, projected onto the plane of rotation of the electric antenna, is indicated by the dashed line in the polar plot of Figure 14.

The angular distribution of electric field strengths is seen to be symmetrically distributed with respect to the magnetic field direction with two distinct maximums when the antenna axis is parallel to the projected magnetic field direction and a minimum when the antenna axis is perpendicular to the static magnetic field. Since only one rotation occurs in the region where the intense electrostatic noise occurs, it is possible that this apparent spin modulation may be due to a coincidental variation of the noise intensity rather than a spin modulation effect. However, the magnetic field gradient, which is expected to be correlated with the electrostatic noise intensity, appears to increase smoothly up to a single maximum and does not indicate a variation associated with the two maximums (at about 1440:40 UT and 1440:46 UT), which occur when the antenna axis is parallel to the magnetic field. Thus it is felt that the angular distribution in the polar plot of Figure 14 is representative of the actual distribution of electric field directions in the shock. Since the magnetic field in this case has an appreciable component perpendicular to the plane of rotation of the electric antenna ($\theta_B = 43°$), we cannot definitely establish that the electric field is aligned parallel to the magnetic field vector, although this is certainly the simplest and most obvious interpretation of the observed modulation. Other similar cases that have been examined usually show definite evidence of spin modulation; however, it is never as pronounced as it is for the upstream plasma oscillations. The modulation factor is usually less than 2 to 1 for maximum and minimum amplitudes, this ratio indicating that wave vector directions of the electrostatic waves in the bow shock are distributed over a relatively broad range of angles. When a definite spin modulation is evident, as it is in Figure 14, the maximum electric field amplitude in the shock usually tends to occur in a direction parallel to the static magnetic field.

Electrostatic turbulence in the magnetosheath. As was previously discussed, a moderate level of electrostatic turbulence is always present in the magnetosheath downstream of the shock. Since the intensity of the magnetosheath electric field noise is usually relatively steady for several rotations of the spacecraft, the electric field direction can be determined with a high degree of confidence in this region. Figure 15 shows the polar plot of a series of rapid-sample measurements obtained in the magnetosheath about 1 min after the shock crossing at 1612:20 UT. These rapid-sample measurements are from the 3.11-kHz electric field channel and include four complete rotations of the spacecraft. The maximum electric field amplitude again occurs when the electric antenna axis is oriented parallel to the static magnetic field direction (projected onto the ecliptic plane). The magnetic field vector in this

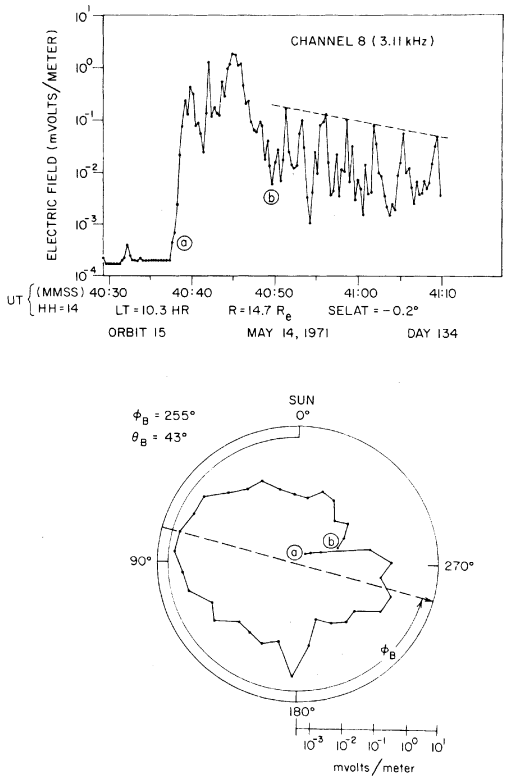

Fig. 14. Rapid-sample measurement of electric field at 3.11 kHz for the bow shock transition and downstream regions. The electric field fluctuations are correlated with magnetic field gradients in both the transition and the downstream region. The polar plot shows the spin modulation of electric field amplitude for the transition region for interval *a* to *b*; ϕ_B is the solar ecliptic longitude of the magnetic field upstream of the shock.

case lies at an angle of $\theta_B = 35°$ above the ecliptic plane. Other similar cases that have been analyzed show that the electric field direction of the magnetosheath turbulence is always oriented nearly parallel to the magnetic field direction. Usually the electric field amplitude perpendicular to the magnetic field is a factor of 3–5 below the amplitude parallel to the magnetic field, indicating that the distribution of electric field directions is rather closely aligned along the static magnetic field direction (within 20° or less).

Summary of Results and Discussion

Upstream of the bow shock, intense narrow band electrostatic plasma oscillations are frequently observed by the Imp 6 plasma wave experiment at frequencies of 10–30 kHz. The spectrum and intensity of these electron plasma oscillations agree with the previous observations of *Fredricks et al.* [1968] and confirm the main features already known about these waves. The Imp 6 spin modulation measurements show that the electric field vector of these plasma oscillations is oriented parallel to the local static magnetic field direction. This electric field direction is consistent with the direction expected if the plasma oscillations are produced by a two-stream instability from electrons that are streaming into the solar wind along magnetic field lines that intersect the shock transition. Broad band electrostatic noise, referred to as a precursor, is also frequently observed by Imp 6 immediately upstream of the shock. This broad band electrostatic noise typically extends from the local electron plasma frequency (which is usually at about 20–30 kHz) down to frequencies of about 1 kHz. The electric field direction of these precursor waves is also oriented parallel to the static magnetic field. Since these precursor waves appear to be closely associated with the long-wavelength narrow band electron plasma oscillations (they have the same electric field polarization, and the upper-frequency limit of the precursor spectrum is the local plasma frequency), it seems most likely that these waves are simply shorter-wavelength electron plasma oscillations that are strongly Doppler shifted downward in frequency from the local plasma frequency. A downward shift in frequency would be expected for waves propagating upstream into the solar wind.

In the shock transition region, two distinct components are evident in the electric field spectrum: one component has a broad peak centered between 200 and 800 Hz, and the other component increases monotonically with decreasing frequency, approximately as $f^{-(2.0\pm0.5)}$. The magnetic field spectrum has only a single component, which increases monotonically with decreasing frequency approximately as $f^{-(4.0\pm0.5)}$. The magnetic field spectrum shows a distinct steepening of the spectrum, indicative of an upper cutoff frequency, at about 100–200 Hz. Since the whistler mode is the only electromagnetic mode that can propagate in this frequency range (above the proton gyrofrequency but below the electron gyrofrequency), this magnetic field turbulence must be caused by whistler mode waves. The steepening of the magnetic field spectrum is thought to be associated with the whistler mode propagation cutoff at the local electron gyrofrequency, which is typically at about 350 Hz in the shock transition region. The monotonic component of the electric field spectrum is thought to be the electric field spectrum of these whistler mode waves. The electric to magnetic field energy density ratio $\epsilon_E/\epsilon_B \simeq 10^{-3}$ to 10^{-4} of the monotonic component is consistent with the electric to magnetic field ratio expected for whistler mode waves. Also the steeper magnetic field spectrum compared with the electric field spectrum is expected because of the increase in the index of refraction, hence in the magnetic to the electric field ratio, with decreasing frequency for the whistler mode in this frequency range.

The broad peak in the electric field spectrum within the shock, centered between 200 and 800 Hz, consists of almost purely electrostatic waves with $\epsilon_E/\epsilon_B \simeq 10^2$ to 10^4. These waves almost certainly correspond to the electrostatic waves discussed by *Fredricks et al.* [1968, 1970*a*, *b*] and *Scarf et al.* [1971], using electric field measurements from Ogo 5. The electrostatic character of these waves, the general frequency range, and their occurrence in association with the magnetic field gradient at the shock transition are in good agreement with the Ogo 5 results. Detailed comparisons of the shape of the frequency spectrum are not possible, since the Ogo 5 data only provide measurements at a single frequency on a given shock crossing. The only area of disagreement concerns the electric field amplitude. Whereas *Scarf et al.* [1970] quote peak electric field strengths for the bow shock of about 30 mV m^{-1} for an equivalent 5-kHz sine wave, the largest peak electric field strength encountered by Imp 6 in this frequency range is about 10 mV m^{-1}. This difference in measured shock electric fields has not been resolved. Electric field spectral densities at 1.3

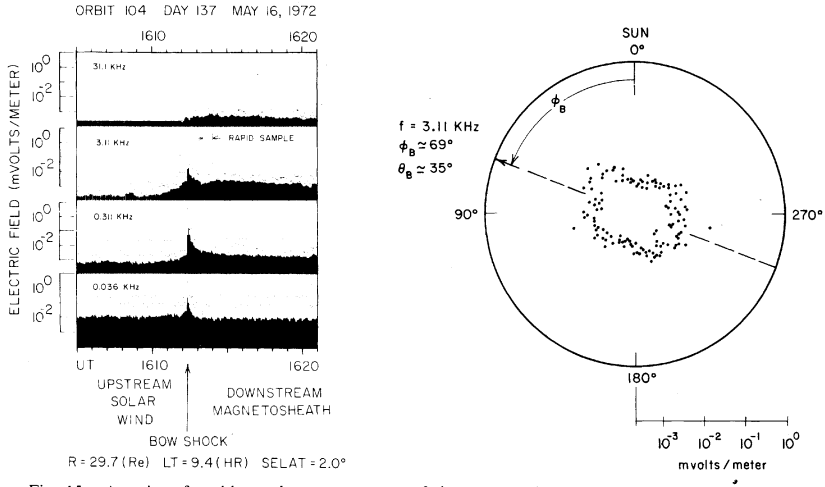

Fig. 15. A series of rapid-sample measurements of the magnetosheath electric field turbulence that shows that the electric field vector of this noise is aligned parallel to the static magnetic field.

kHz reported by *Fredricks et al.* [1970*b*] in the discussion of their Figure 4, p. 3757, that result in electric field strengths an order of magnitude greater than Imp 6 measurements are a typographical error (F. L. Scarf, personal communication, 1974). One possible explanation for the different electric fields measured is that the wavelength of the electrostatic waves may be much shorter than the length of the long electric antennas on Imp 6. However, sufficiently short wavelengths (~10 m) to account for such a large error would have a Doppler shift (~10 kHz) too large to account for the low frequency (200–800 Hz) at which the peak in the spectrum occurs. Also comparisons between the two long antennas on Imp 6, which have different lengths, give consistent results, and cross calibrations with the magnetic antennas, using electromagnetic waves with a known electric to magnetic field ratio, give consistent results [*Gurnett and Shaw,* 1973]. Further studies are being conducted, using the short electric antenna on Imp 6, which is similar to the short electric antenna on Ogo 5, to determine the reason for this apparent disagreement in the peak electric field amplitudes.

The Imp 6 spin modulation measurements show that the electric field directions of the electrostatic waves in the bow shock tend to be oriented parallel to the static magnetic field. Since only one rotation is normally available in the shock transition region, this result is not as reliable for the upstream electron plasma oscillations, where many rotations are usually available. However, sufficient cases have been examined that one can be reasonably confident of the electric field orientation in the transition region. This electric field orientation is consistent with the electric field directions expected for ion sound waves propagating along the magnetic field direction [*Tidman and Krall,* 1971] and is inconsistent with the electric field directions expected for the Bernstein mode turbulence suggested by *Gary and Sanderson* [1970], *Wu and Fredricks* [1972], and others.

In the magnetosheath downstream of the shock a moderate level of electrostatic turbulence is always present. This electrostatic turbulence has a spectrum that is similar to that of the electrostatic turbulence in the shock transition region but has an electric field strength about 1–2 orders of magnitude smaller than that of the spectrum in the transition region. The spin modulation measurements show that the electric field direction of this turbulence is also oriented parallel to the static magnetic field. The similarity of the spectrum and the electric field direction of electrostatic turbulence in the bow shock and in the magnetosheath suggests that the same instability mechanism may be operative in both these regions, the intensity of the turbulence being roughly proportional to the diamagnetic currents and magnetic field gradients that occur in these two regions.

Acknowledgments. We wish to extend our thanks to N. Ness and D. Fairfield for providing the Imp 6 magnetic field data used in this study and to R. Shaw, G. Voots, R. West, and W. Kurth for their assistance in the data analysis. This work was supported in part by the National Aeronautics and Space Administration under contracts NAS5-11074 and NAS5-11431 and grant NGL-16-001-043 and by the Office of Naval Research under grant N00014-68-A-0196-0009.

The Editor thanks R. W. Fredricks and R. E. Holzer for their assistance in evaluating this paper.

REFERENCES

Fairfield, D. H., Average and unusual locations of the earth's magnetopause and bow shock, *J. Geophys. Res., 76,* 6700, 1971.

Formisano, V., and P. C. Hedgecock, Solar wind interaction with the earth's magnetic field, 3, On the earth's bow shock structure, *J. Geophys. Res., 78,* 3745, 1973*a*.

Formisano, V., and P. C. Hedgecock, On the structure of the turbulent bow shock, *J. Geophys. Res., 78,* 6522, 1973*b*.

Fredricks, R. W., C. F. Kennel, F. L. Scarf, G. M. Crook, and I. M. Green, Detection of electric-field turbulence in the earth's bow shock, *Phys. Rev. Lett., 21,* 1761, 1968.

Fredricks, R. W., F. V. Coroniti, C. F. Kennel, and F. L. Scarf, Fast time-resolved spectra of electrostatic turbulence in the earth's bow shock, *Phys. Rev. Lett., 24,* 994, 1970*a*.

Fredricks, R. W., G. M. Crook, C. F. Kennel, I. M. Green, and F. L. Scarf, Ogo 5 observations of electrostatic turbulence in bow shock magnetic structures, *J. Geophys. Res., 75,* 3751, 1970*b*.

Fredricks, R. W., F. L. Scarf, and L. A. Frank, Nonthermal electrons and high-frequency waves in the upstream solar wind, 2, Analysis and interpretation, *J. Geophys. Res., 76,* 6691, 1971.

Fredricks, R. W., F. L. Scarf, and I. M. Green, Distributions of electron plasma oscillations upstream from the earth's bow shock, *J. Geophys. Res., 77,* 1300, 1972.

Gary, S. P., and J. J. Sanderson, Longitudinal waves in a perpendicular collisionless plasma shock, 1, Cold ions, *J. Plasma Phys., 4,* 739, 1970.

Gurnett, D. A., and R. R. Shaw, Electromagnetic radiation trapped in the magnetosphere above the plasma frequency, *J. Geophys. Res., 78,* 8136, 1973.

Holzer, R. E., M. G. McLeod, and E. J. Smith, Preliminary results from the Ogo 1 search coil magnetometer: Boundary positions and magnetic noise spectra, *J. Geophys. Res., 71,* 1481, 1966.

Holzer, R. E., T. G. Northrup, J. V. Olson, and C. T. Russell, Study of waves in the earth's bow shock, *J. Geophys. Res., 77,* 2264, 1972.

Montgomery, M. D., J. R. Asbridge, and S. J. Bame, Vela 4 plasma observations near the earth's bow shock, *J. Geophys. Res., 75,* 1217, 1970.

Olson, J. V., R. E. Holzer, and E. J. Smith, High-frequency magnetic fluctuations associated with the earth's bow shock, *J. Geophys. Res., 74,* 4601, 1969.

Scarf, F. L., R. W. Fredricks, and C. F. Kennel, AC electric and magnetic fields and collisionless shock structures, in *Particles and Fields in the Magnetosphere,* edited by B. M. McCormac, p. 102, D. Reidel, Dordrecht, Netherlands, 1970.

Scarf, F. L., R. W. Fredricks, L. A. Frank, and M. Neugebauer, Nonthermal electrons and high-frequency waves in the upstream solar wind, 1, Observations, *J. Geophys. Res., 76,* 5162, 1971.

Tidman, D. A., and N. A. Krall, *Shock Waves in Collisionless Plasmas,* p. 118, Interscience, New York, 1971.

Wu, C. S., and R. W. Fredricks, Cyclotron drift instability in the bow shock, *J. Geophys. Res., 77,* 5585, 1972.

(Received April 15, 1974;
accepted September 25, 1974.)